Antifriction Bearings Damage Analysis Using Experimental Data Based Models

R. G. Desavale
e-mail: ramdesavale@rediffmail.com

R. Venkatachalam
e-mail: chalamrv@yahoo.com

Department of Mechanical Engineering,
National Institute of Technology,
Warangal 506 004, Andra Pradesh, India

S. P. Chavan
Department of Mechanical Engineering,
Walchand College of Engineering,
Sangli 416 415, Maharashtra, India
e-mail: chavan.walchand@gmail.com

Diagnosis of antifriction bearings is usually performed by means of vibration signals measured by accelerometers placed in the proximity of the bearing under investigation. The aim is to monitor the integrity of the bearing components, in order to avoid catastrophic failures, or to implement condition based maintenance strategies. In particular, the trend in this field is to combine in a simple theory the different signal-enhancement and signal-analysis techniques. The experimental data based model (EDBM) has been pointed out as a key tool that is able to highlight the effect of possible damage in one of the bearing components within the vibration signal. This paper presents the application of the EDBM technique to signals collected on a test-rig, and be able to test damaged fibrizer roller bearings in different working conditions. The effectiveness of the technique has been tested by comparing the results of one undamaged bearing with three bearings artificially damaged in different locations, namely on the inner race, outer race, and rollers. Since EDBM performances are dependent on the filter length, the most suitable value of this parameter is defined on the basis of both the application and measured signals. This paper represents an original contribution of the paper. [DOI: 10.1115/1.4024638]

Keywords: antifriction bearings, experimental data based models, dimensional analysis, condition based maintenance, defects, FFT analyzer, Buckingham theorem

1 Introduction

Bearings are mechanical components largely used in rotating machines and employed in many industrial fields. It is observed that due to the load applied and the harsh operating environment, bearings are prone to fail and may even lead to catastrophic failure of the machinery. Typical failures of rolling bearings are due to cracks or spalls on rolling elements, inner ring and/or outer ring, and seldom on the cage. A proper diagnostics of bearings during their functioning must be performed to avoid catastrophes. Diagnosis of bearing is usually performed by processing the vibration signals measured by means of transducers placed on the bearing pedestals. Signal processing techniques have been implemented for this purpose. The autopower spectrum is probably the most established technique, which was proposed for the first time [1] which allows detection of the frequencies related to faults of bearings. Similar information is provided by the spectral kurtosis, wherein a distribution in frequency domain is also obtained [2,3]. The reliability of the cyclostationary analysis for bearings diagnostics has been tested in several applications. Frequency components strictly related to the fault presence could be traced in the frequency plane. The application of these techniques is necessary for bearing diagnostics, but their effectiveness is often reduced by both environmental noise and other vibration sources. For this reason, often it is useful to enhance the measured vibration signals in order to highlight components due to faults. The purpose of this paper is to provide a brief, but effective, introduction to the Buckingham theorem (BT), so that more researchers could get familiar with its functioning, appreciate its enormous capabilities in supporting model development and empirical analysis, and eventually include the BT into their "researcher's toolbox" [4]. An example of experimental data based models is represented by dimensional analysis (DA). The DA, proposed for the first time for the study of vibration signals, has been recently considered in the mechanical field.

In this paper, DA is applied to vibration signals measured on a test-rig which is able to test sugar industrial roller bearings. Signals were acquired on undamaged and damaged bearings at different working conditions. The aim is to investigate the effectiveness of the DA on experimental signals.

2 Literature Review

Patel et al. [5] reported a dynamic model for the study of vibrations of deep groove ball bearings having single and multiple defects on surfaces of inner and outer races. Masses of shaft, housing, races, and balls were considered in the modeling. The coupled solution of governing equations of motions was obtained using the Runge–Kutta method. The model provides the vibrations of shaft, balls, and housing in time and frequency domains. Computed results from the model were validated with experimental results, which were generated using healthy and defective deep groove ball bearings. Characteristic defect frequencies and its harmonics were broadly investigated using both theoretical and experimental results. Comparison of vibration spectra for the cases having single and two defects on races reveals relatively higher velocity amplitudes with two defects. Good correlations between theoretical and experimental results were observed. The authors believe that this dynamic model can be used with confidence for the study and prediction of vibrations of healthy and defective deep groove ball bearings.

Patil et al. [6] presented an analytical model for predicting the effect of a localized defect on the ball bearing vibrations. In the analytical formulation, the contacts between the ball and the races are considered as nonlinear springs. The contact force was calculated using the Hertzian contact deformation theory. A computer program was developed to simulate the defect on the raceways with the results presented in the time domain and frequency domain. Shuang [7] proposed an analysis method of a combination of wavelet analysis and chaos. In their method, wavelet

Contributed by the Tribology Division of ASME for publication in the JOURNAL OF TRIBOLOGY. Manuscript received September 12, 2012; final manuscript received April 16, 2013; published online August 6, 2013. Assoc. Editor: Xiaolan Ai.

Table 1 Summary of work related to antifriction bearings

Sr. no.	Approaches (theories and methodologies studied)	Loading type/condition	References
1	time-domain analysis, frequency response analysis, statistical analysis	outer race fault, inner race fault	[2,3,9–11,27]
2	chaotic vibration analysis, acoustic emission monitoring	outer, inner race	[26,28,29]
3	mathematical model	Single and multiple defects	[5,8,30–40]
4	auto-power spectrum and cross-power spectrum	outer race, inner race	[1]
5	bond graphs	outer, inner race	[12]
6	taguchi method	outer, inner race	[13]
7	envelop analysis	outer, inner race	[41]
8	correlation dimension and bispectra	outer, inner race	[14,42]
9	modal analysis	outer, inner race	[43]
10	neural networks and wavelet analysis	outer, inner race	[7,15–25]
11	dimensional analysis (EDBM)	single defect and multiple defects	[—]

analysis was first adopted to conduct denoising preprocessing to the signals analyzed and the fault information components of the bearing were detected out effectively. Then by calculating chaotic characteristics, such as the correlation dimension of rolling bearing vibration time series, motion state features of equipment were extracted and a detailed analysis was carried out. The results show that the method could realize fault diagnosis of rolling bearing, thus providing a new approach to fault diagnosis of rotating machinery.

Arslan and Aktürk [8] developed a shaft-bearing model in order to investigate the rolling element vibrations for an angular contact ball bearing with and without defects. The shaft-bearing assembly was considered as a mass-spring system. The system shows a nonlinear characteristic under dynamic conditions. The equations of motion in radial and axial directions were obtained for shaft and rolling elements, and they were solved simultaneously with a computer simulation program. Additionally, the effect of localized defects on running surfaces (i.e., inner ring, outer ring, and ball) on the vibration of the balls was investigated. The vibration of the rolling elements in the radial direction was analyzed in time and frequency domains. Characteristic defect frequencies and their components could be seen in the frequency spectra of rolling element vibrations. Comparison of the obtained results with similar studies available in literature showed reasonable qualitative agreement.

From the literature review of around 50 reference papers on investigation of rolling element vibrations, the following are observed. Many papers [2,3,9–11] have carried out bearing vibration response analysis in time domain and frequency domain and the results have been presented in statistical form. In these papers, the defect(s) on inner and/or outer race have been considered. A few papers have given the methods of chaotic vibration analysis and acoustic emission monitoring. In these papers the defect(s) on inner and/or outer race have been considered. A paper by Massimo and Alberto [1] described a method of analysis using the auto-power spectrum and cross-power spectrum. In this paper the defect(s) on inner and/or outer race have been considered.

A paper by Michael [12] described the method analysis using bond graphs. In this paper the defect(s) on inner and or outer race were considered. A paper by Ahmet and Jagannathan [13] described the method of analysis using the Mahalanobis-Taguchi system (MTS) as a prognostics tool. In this paper, the defect(s) on inner and/or outer race were considered. A few papers [14] gave the methods by using the correlation dimension and Bispectra. In these papers the defect(s) on inner and/or outer race were considered. Recently a large number of papers [7,15–25] have applied the wavelet-neural network, neural network, and wavelet analysis for the bearing vibration response analysis. In these papers the defect(s) on inner and/or outer race were considered.

From these reviews of research papers, it is seen that there is a scope for the investigation of vibration response of rolling element bearing in a rotor by using the method of bond graph and or dimensional analysis (experimental data based model method using DA). A summary of work related to antifriction bearings studied on various loading types, as well as conditions by different researchers in the laboratory, is provided in Table 1.

In light of the above-mentioned points one can propose to carry out some studies on vibration responses of antifriction bearing in a rotor bearing system, under single and or multiple defects of inner and/or outer race of the rings. For this purpose, the experimental data based modeling (EDBM) method using dimensional analysis (DA) is proposed.

3 Equations of Motion of the Rotor-Bearing System

Since the models have enough characteristics for changing data, we can study the effect of input parameters on vibration amplitude characteristic by graphs on the basis of models and predict response change values on the surface of the input. In order to use the experimental data based method we need to calculate the lateral vibration characteristics of the rotor-bearing system (Fig. 1). The entire system is modeled with the rotor element, bearing element, and shaft element. The object of this section is to introduce the parameters of these elements and the equations of motion of the entire rotor-bearing system. The element property matrices of the rotor element, bearing element, and shaft element can be assembled by means of the conventional finite element assembly technique [26], to form the equations of motion of the entire rotor-bearing system,

$$M\ddot{u} + C\dot{u} + Ku = F(t) \tag{1}$$

where $\{u\}$, $\{\dot{u}\}$, and $\{\ddot{u}\}$ are the displacement, velocity, and acceleration vectors, respectively, $[M]$, $[C]$, and $[K]$ are the overall mass, damping, and stiffness matrices, respectively, while $\{F(t)\}$ is the external force vector of the entire rotor-bearing system. The element damping matrices of the rotor and shaft elements depend

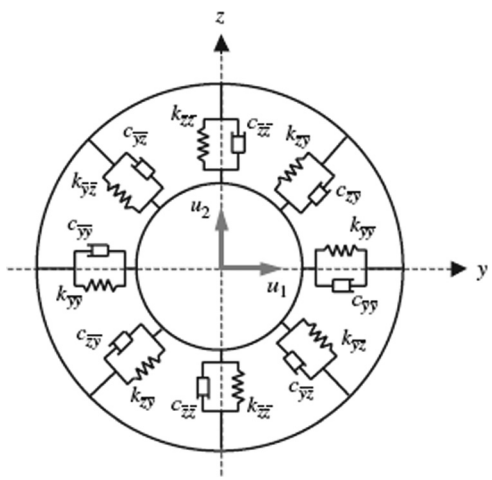

Fig. 1 Mathematical model of the antifriction bearing

on the rotating speed of the rotor. The overall damping matrix, [*C*], of the entire rotor-bearing system is dependent on the rotating speed of the rotor.

4 Mathematical Developments

The aim of the EDBM analysis is to find the expressions of the dimensional analysis under dynamic conditions for the rotor-bearing systems, so that the physical characteristics (such as natural frequencies, displacements, velocities, and/or forces can be used to predict the system). In this work, an analytical model is proposed for estimating the vibration amplitude in antifriction bearing by using the concepts of dimensional analysis, including the parameters below. Knowing the governing parameters of the physical problem and by using the concepts of experimental data based models, a relationship is obtained between different parameters involved. The first task is to identify a relevant set of bearing variables. The set should be "complete," such that none of the independent variables can be derived from others, while the dependent variables can be derived [4]. The independent variables relate to bearing geometry, operating conditions, and materials properties. In this study, the dependent variables are load and speed. A suitable set of variables are given in Table 1. A mass-length-time (MLT) unit reference set is used.

According to the numerical model of antifriction bearing proposed in this paper, the functional relationship is the following. The vibration amplitude *A* can be given by an equation of the form,

$$\text{Amplitude } (A) = f\left(\begin{matrix} D, d_b, d_i, d_o, d_m, Z, C_r, d_{gi}, d_{go}, \theta_i, H_d, l_r, B, n_d, N_s, W, \\ K, C, \eta, T_f, m_r, m_i, m_o, m_b, S, \delta, E, \rho, \nu, f_c, f_b, f_{id}, f_{od}, f_{bd} \end{matrix}\right) \tag{2}$$

where *f* is an unknown function, assuming that this function is in the form of a product of powers. The number of dimensionless products in a complete set is equal to the total number of variables minus the maximum number of these variables that will not form a dimensionless product. Therefore, the number of independent group will be m, according to Buckingham (π) theorem the number of independent dimensionless (π)-products is given by the equation (3).

According to Buckingham's ''π'' theorem, the number of independent dimensionless π-products is (36 variables) – (3 reference dimensions) = 33 π-terms,

$$\begin{aligned} m &= n - r \\ &= 36 - 3 = 33 \end{aligned} \tag{3}$$

It may be assumed that the vibration amplitude depends on the speed, radial load, and density of material, lubricant viscosity, stiffness and damping, and temperature. In antifriction bearing, speed and load has a significant role to play in changing the vibration amplitude. The dimensions of all these quantities are reported in the *M, L, T, θ* system as shown in Table 2. All of the above variables considered for the problem are assembled using Buckingham's π theorem (BT) in a number of dimensional products (π_i) as follows [4].

That is, we have

$$f(\pi_1, \pi_2, \pi_3, \pi_4, \pi_5, \pi_6, \ldots, \pi_{m-n}) = 0$$

where *f* is some function, or in an alternate expression,

$$\pi_1 = f(\pi_2, \pi_3, \pi_4, \pi_5, \pi_6, \ldots, \pi_{m-n}) \tag{4}$$

In the lower part of Table 3, according to the procedure, the formulation of the dimensionless numbers is obtained. In this regard, as we anticipated above, the BT does not give any hint concerning the form of the new equation, or the best dimensionless set to be developed out of the starting dimensional variables. This will allow a better experimental control, and simplify the search of the functional form of the dimensionless equation.

Table 2 Units and dimensions of variables/parameters

Parameters/variables	Symbols	SI units	Dimensions (SI) MLT θ system
(*a*) Geometrical parameters			
Bore diameter	D	*m*	(*L*)
Ball/roller diameter	d_b	*m*	(*L*)
Inner race diameter	d_i	*m*	(*L*)
Outer race diameter	d_o	*m*	(*L*)
Pitch diameter	d_m	*m*	(*L*)
No. of balls/rollers	Z	—	—
Radial clearance	C_r	*m*	(*L*)
Inner groove diameter	d_{gi}	*m*	(*L*)
Outer groove diameter	d_{go}	*m*	(*L*)
Initial position of the defect	θ_i	—	—
Height of defect (size)	H_d	*m*	(*L*)
Length of roller	L_r	*m*	(*L*)
Bearing width	B	*m*	(*L*)
No. of defects	n_d	—	—
(*b*) Physical parameters			
Speed of shaft	N_S	rpm	(T^{-1})
Radial load	W	N	(MLT^{-2})
Spring constant	K	N/m	(MT^{-2})
Damping	C	N S/m	(MT^{-1})
Lubricant viscosity	H	N s/m^2	($ML^{-1}T^{-1}$)
Resisting torque (frictional)	T_F	N m	(ML^2T^{-2})
Mass of rotor	m_r	kg	(Mr)
Mass of the inner race	m_i	kg	(Mi)
Mass of the outer race	m_o	kg	(Mo)
Mass of the ball/roller	m_b	kg	(Mb)
Stresses	S	N/m^2	($ML^{-1}T^{-2}$)
Deflection	δ	M	(L)
Cage frequency	f_c	Hz (r/min)	(T^{-1})
Ball spinning frequency	f_b	Hz (r/min)	(T^{-1})
Inner race defect frequency	f_{id}	Hz (r/min)	(T^{-1})
Outer race defect frequency	f_{od}	Hz (r/min)	(T^{-1})
Ball defect frequency	f_{bd}	Hz (r/min)	(T^{-1})
(*c*) Material parameters			
Young's modulus	E	N/m^2	($ML^{-1}T^{-2}$)
Density of bearing material	ρ	kg/m^3	(ML^{-3})
Poisson's ratio	ν	—	($M^0L^0T^0$)= 1
Coefficient of friction	μ	—	($M^0L^0T^0$)= 1
(*d*) Response parameters			
Vibration amplitude	A	Mm	(L)

4.1 Reductions of Dimensionless Forms. The observation that a dimensionally homogeneous equation among several variables can be reduced to an equation among a smaller number of dimensionless variables is principally due to Rayleigh and Buckingham. For each of the problems, it can be shown that the two π terms combine to form the high-level dimensionless variables as follows:

$$\pi_a = \frac{\pi_2}{\pi_5} = \frac{d_b}{D} \cdot \frac{D}{d_m} = \frac{d_b}{d_m} \tag{5}$$

$$\pi_b = \frac{\pi_3}{\pi_4} = \frac{d_i}{D} \cdot \frac{D}{d_o} = \frac{d_i}{d_o} \tag{6}$$

$$\pi_c = \frac{\pi_7}{\pi_{12}} = \frac{C_r}{D} \cdot \frac{D}{l_r} = \frac{C_r}{l_r} \tag{7}$$

$$\pi_d = \frac{\pi_{11}}{\pi_{13}} = \frac{H_d}{D} \cdot \frac{D}{B} = \frac{H_d}{B} \tag{8}$$

$$\pi_e = \frac{\pi_9}{\pi_8} = \frac{d_{go}}{D} \cdot \frac{D}{d_{gi}} = \frac{d_{go}}{d_{gi}} \tag{9}$$

Table 3 Dimensionless π terms for antifriction bearings

Sr. no.	Π_i	Estimated Π terms
1	Π_1	$\frac{a_o}{D}$
2	Π_2	$\frac{d_b}{D}$
3	Π_3	$\frac{d_i}{D}$
4	Π_4	$\frac{d_o}{D}$
5	Π_5	$\frac{d_m}{D}$
6	Π_6	Z
7	Π_7	$\frac{C_r}{D}$
8	Π_8	$\frac{d_{gi}}{D}$
9	Π_9	$\frac{d_{go}}{D}$
10	Π_{10}	θ_i
11	Π_{11}	$\frac{H_d}{D}$
12	Π_{12}	$\frac{l_r}{D}$
13	Π_{13}	$\frac{B}{D}$
14	Π_{14}	n_d
15	Π_{15}	$\frac{KD}{W}$
16	Π_{16}	$\frac{CND}{W}$
17	Π_{17}	$\frac{\eta D^2 N}{W}$
18	Π_{18}	$\frac{T_f}{WD}$
19	Π_{19}	$\frac{m_r DN^2}{W}$
20	Π_{20}	$\frac{m_i DN^2}{W}$
21	Π_{21}	$\frac{m_o DN^2}{W}$
22	Π_{22}	$\frac{m_b DN^2}{W}$
23	Π_{23}	$\frac{SD^2}{W}$
24	Π_{24}	$\frac{\delta}{W}$
25	Π_{25}	$\frac{f_c}{N}$
26	Π_{26}	$\frac{f_b}{N}$
27	Π_{27}	$\frac{f_{id}}{N}$
28	Π_{28}	$\frac{f_{od}}{N}$
29	Π_{29}	$\frac{f_{bd}}{N}$
30	Π_{30}	$\frac{ED^2}{W}$
31	Π_{31}	$\frac{\rho D^4 N^2}{W}$
32	Π_{32}	υ
33	Π_{33}	μ

$$\pi_f = \frac{\pi_{19}}{\pi_{22}} = \frac{m_r DN^2}{W} \cdot \frac{W}{m_b DN^2} = \frac{m_r}{m_b} \tag{10}$$

$$\pi_g = \frac{\pi_{21}}{\pi_{20}} = \frac{m_o DN^2}{W} \cdot \frac{W}{m_i DN^2} = \frac{m_o}{m_i} \tag{11}$$

$$\pi_h = \frac{\pi_{15}}{\pi_{16}} = \frac{KD}{W} \cdot \frac{W}{CND} = \frac{K}{CN} \tag{12}$$

$$\pi_i = \frac{\pi_{17}}{\pi_{18}} = \frac{\eta D^2 N}{W} \cdot \frac{WD}{T_f} = \frac{\eta D^3 N}{T_f} \tag{13}$$

$$\pi_j = \frac{\pi_{23}}{\pi_{24}} = \frac{SD^2}{W} \cdot \frac{D}{\delta} = \frac{SD^3}{\delta W} \tag{14}$$

$$\pi_k = \frac{\pi_{30}}{\pi_{31}} = \frac{ED^2}{W} \cdot \frac{D}{\rho D^4 N^2} = \frac{E}{\rho D^2 N^2} \tag{15}$$

$$\pi_l = \pi_h . \pi_i = \frac{K}{CN} \cdot \frac{\eta D^3 N}{T_f} = \frac{K \eta D^3}{C T_f} \tag{16}$$

$$\pi_m = \frac{\pi_k}{\pi_j} = \frac{\rho D^2 N^2}{E} \cdot \frac{\delta W}{SD^3} = \frac{\rho N^2 \delta W}{ESD} \tag{17}$$

$$\pi_n = \frac{\pi_{26}}{\pi_{25}} = \frac{f_b}{f_c} \tag{18}$$

$$\text{Constant} = \beta = \left(\pi_a . \pi_b . \pi_c . \pi_d . \pi_e . \pi_f . \pi_g . Z . \theta i . n_d . \upsilon . \mu\right) \tag{19}$$

$$\text{Constant} = \beta = (Z . \theta_i . n_d . \upsilon . \mu) . \left(\frac{d_b}{d_m} . \frac{d_i}{d_o} . \frac{d_{go}}{d_{gi}}\right) . \left(\frac{C_r}{l_r} . \frac{H_d}{B}\right) . \left(\frac{m_r}{m_b} . \frac{m_o}{m_i}\right) \tag{20}$$

The above parameters are constants for motion of a rolling element bearing. The complete formula of the vibration amplitude evaluation criterion has the following form: detailed mathematical analysis shows that

$$\frac{a_0}{D} = A = f\left(\beta, \frac{1}{Z}, n_d, \frac{C_r}{l_r}, \frac{H_d}{B}, \frac{K \eta D^3}{C T_f}, \frac{\rho N^2 \delta W}{ESD}, \frac{f_b}{f_c}, \frac{f_{id}}{N_s}, \frac{f_{od}}{N_s}, \frac{f_{bd}}{N_s}\right) \tag{21}$$

Equation (21) shows the model for predictions and calculating defects, vibration amplitude and defect size, Fig. 2.

Henceforth, f written without a subscript indicates a functional relationship between dependent and independent variables,

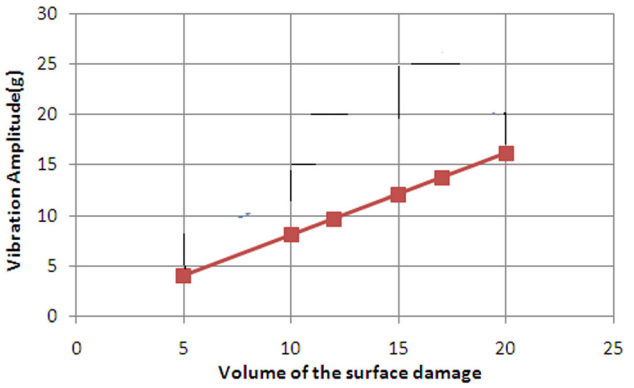

Fig. 2 Dimensionless relationships between vibration amplitudes versus surface damage

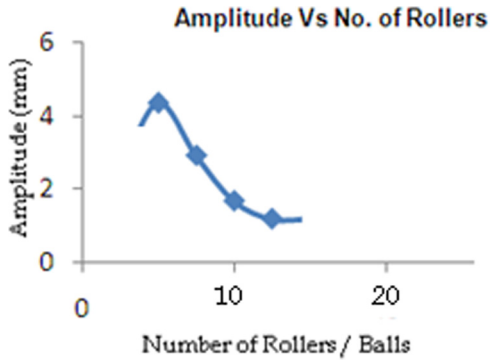

Fig. 3 Variation of amplitude with number of rollers

Table 4 Vibration of defective bearing (before balancing)

Location	Displacement P-P microns	Peak micron	Velocity rms m/s^2	Acceleration (P) m/s^2
UGB-H	53.138	25.69	1.229	0.908
UGB-V	50.591	24.67	1.199	0.845
UGB-A	7.591	3.340	0.226	0.217
LGB-H	16.34	7.807	0.524	0.578
LGB-V	16.06	8.271	0.461	0.557
LGB-A	8.206	3.658	0.268	0.679
TGB-H	1.705	0.636	0.067	0.801
TGB-V	1.341	0.636	0.049	0.917
TGB-A	1.992	—	0.094	0.656

Table 5 Vibration of bearing (after balancing)

Location	Displacement P-P microns	One time peak in micron	Velocity in rms m/s^2	Acceleration peak m/s^2
UGB-H	7.505	3.340	0.238	0.939
UGB-V	7.145	3.499	0.231	0.898
UGB-A	3.450	1.431	0.181	0.253
LGB-H	2.064	0.636	0.094	0.454
LGB-V	1.977	0.954	0.098	0.451
LGB-A	2.157	0.636	0.155	0.400
TGB-H	1.260	—	0.057	1.329
TGB-V	1.624	0.636	0.055	1.663
TGB-A	1.397	—	0.090	0.963

without specifying the particular function for such relationship. The form of the function, f, must be determined experimentally.

5 Results and Discussions

5.1 Effects of the Number of Rollers. The vibration amplitude is defined in Eq. (21) and it shows that, vibration amplitude (A) is proportional to stiffness of the bearing (K) and vibration amplitude (A) is inversely proportional to the number of rollers (Z), Fig. 3. Increasing the number of balls/rollers means increasing the number of balls supporting the shaft, therefore increasing the system stiffness and reducing the vibration amplitude. Unbalance response data were presented for a rotor supported on bearings with accurate bearing stiffness as a function of speed and load. Bearing stiffness was found to be a strong function of bearing deflection, with higher deflection producing markedly higher stiffness. Rotor dynamic analysis showed that unbalance response varied nonlinearly with the amount of rotor imbalance. Moreover, the increase in bearing stiffness as critical speeds were approached, caused a large increase in rotor and bearing vibration

Table 6 Vibration bearings (after excitation)

Location	Displacement P-P microns	One time peak in micron	Velocity in rms m/s^2	Acceleration peak m/s^2
UGB-H	13.63	6.203	0.409	0.909
UGB-V	13.25	6.279	0.305	0.868
UGB-A	2.503	—	0.135	0.260
LGB-H	3.170	1.113	0.122	0.598
LGB-V	2.948	0.795	0.140	0.596
LGB-A	3.724	0.477	0.165	0.521
TGB-H	1.385	0.318	0.060	1.825
TGB-V	1.505	—	0.050	1.773
TGB-A	1.360	—	0.150	1.230

Table 7 Vibration bearings at full load

Location	Displacement P-P microns	One time peak in micron	Velocity in rms m/s^2	Acceleration peak m/s^2
UGB-H	12.63	6.203	0.453	1.770
LGB-H	3.456	1.272	0.458	1.722
TGB-H	1.131	0.477	0.142	5.295

Table 8 Adding weight at 183°

Location	Displacement P-P microns	One time peak in micron	Velocity in rms m/s^2	Acceleration peak m/s^2
UGB-H	12.05	6.279	0.401	1.015
LGB-H	2.172	0.636	0.124	0.508
TGB-H	1.199	—	0.073	1.015

Table 9 Full load vibration readings

Location	Displacement P-P microns	One time peak in micron	Velocity in rms m/s^2	Acceleration peak m/s^2
UGB-H	10.15	1.454	0.740	4.073
LGB-H	4.906	0.636	1.266	6.073
TGB-H	2.152	0.318	0.444	12.38

amplitude over part of the speed range, compared to the case of constant stiffness bearings (see Tables 4–10).

5.2 Effect of Damping. From Fig. 4 vibration amplitude is inversely proportional to damping (C). Damping reduces the amplitude of vibrations. Energy levels of defect frequencies in general, increase as the speed of operation increase to the maximum operating speed.

5.3 Effect of the Number of Defects. From the theoretical graph from Eq. (21), Fig. 5 shows that the amplitude is proportional to the number of defects (n_d). (Outer race/inner race defect size, there is a significant increase in the magnitude levels with the increase in load. There is a large variation in amplitude for various positions of defect under radial load condition.)

5.4 Effect of Radial Clearance. From Eq. (21) it demonstrates the radial clearance on the force/displacement responses shown as the amplitude increases, the horizontal displacement response is the highest, due to an increase in radial clearance. For the horizontal displacement the most dominant frequency is the roller passing frequency, which is the multiplication of the cage frequency and the number of roller pairs. Due to radial clearance,

Table 10 Vibration readings (online condition monitoring systems)

Location	Commissioning time reading		Initial readings at no load before balancing		After balancing at 70 MW load		After fine balancing at no load		After fine balancing at full load after 1 h	
	IRD in μm	BNC in mils	IRD in μm	BNC in mils	IRD in μm	BNC in mils	IRD in μm	BNC in mils	IRD in μm	BNC in mils
UGB	28	1.25	65	5	51	2.9	55	2.5	40	2.5
LGB	50	2.0	140	7	18	3.2	12	2.5	20	3.5
TGB	60	2.5	—	2.5	—	1.5	—	—	—	2.5

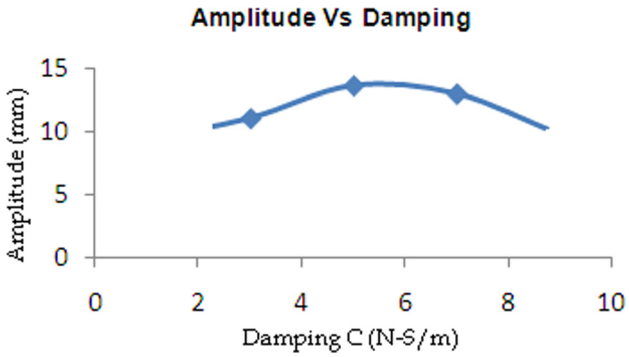

Fig. 4 Dimensionless variation of amplitude versus damping

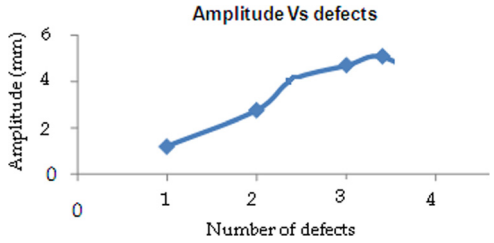

Fig. 5 Variation of amplitude with defects

the major response peaks mostly appear at the high harmonics of the roller passing frequency.

5.5 Effect of Load. From Eq. (21), the correlation between the preload and system vibrations has not been quantified so far. This issue is addressed in this section. It is obvious that load does increase the overall vertical force response as results of an increase in the amplitude of vibration. The overall response magnitudes decrease about 20%–30% from the nonpreload case. More interesting results are observed for the axial load conditions. In addition to affecting vibration, the speed of a rotating machine can also affect the progression of a bearing fault. When rotating machines are operated continuously at a constant speed, the increase in rotating machinery vibration due to a developing bearing fault is approximately monotonic [6]. This is in contrast to bearings that are operated at various speeds throughout their lifetime. Since changing the speed significantly affects the overall machine vibrations, changing the speed can also affect the rate of development of the bearing fault.

5.6 Effect of Speed. The speed of a rotating machine can potentially be one of the most significant factors affecting the machine vibration. If the machine is driven by an electronic converter, the speed is controlled directly by the drive. If the machine is a line-connected induction machine (the most prevalent rotating machine type in the industry), the speed is determined by the load

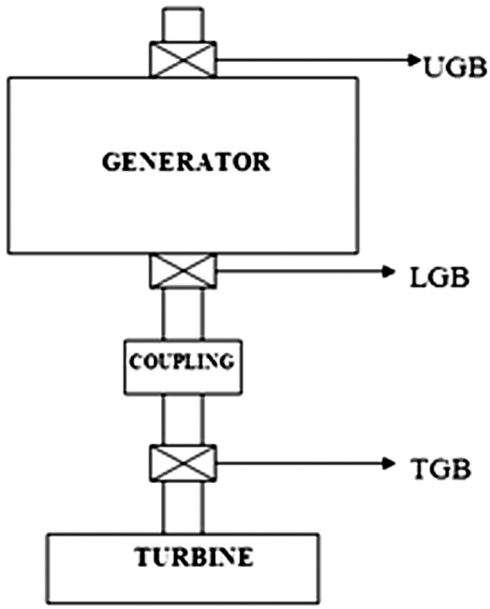

Fig. 6 Experimental setup

level. In either case, the rotating machine speed can change continuously, and this relationship between speed and vibration is often neglected in many bearing condition monitoring schemes. A rotating machine and all of its coupled masses will exhibit a given mechanical frequency response with areas of damping or resonance at given speeds. As the speed of the rotating machine changes, the operating point of the rotating machine will move throughout these regions of increased damping or resonance. This principle contributes to deviations in machine vibration resulting from variations in speed. When the rotating machine and its bearings are healthy, these deviations in vibration are less pronounced and usually go unnoticed. However, as bearing health degrades these deviations in rotating machine vibration due to speed becomes quite significant.

6 Experimentations

The experimental setup used for dynamic analysis of antifriction bearings study is shown in Fig. 6. It consists of a shaft supported on three bearings and driven by a turbine. The test bearing, a double-row spherical bearing SKF 23l52 CCK/W33, adaptor sleeve H3152A, lock nut HM52T, locking washer MB52, NDE-curb bearing C3152 K/C3, bearing pedestal GFO-3104, quantity 2 Nos. (oil cooled), clearance between turbine shaft and generator shaft 5 mm, and roller bearings radial residual clearance 0.14–0.20 mm, turbine generator coupling gear type, No. AFG MAP 109 124, is placed on the nondrive end of the shaft and a double-row self-aligning roller bearing is placed on the drive end side. A piezo-electric accelerometer with a sensitivity of 100 mV/g is used to measure the vibrations. It is mounted on the

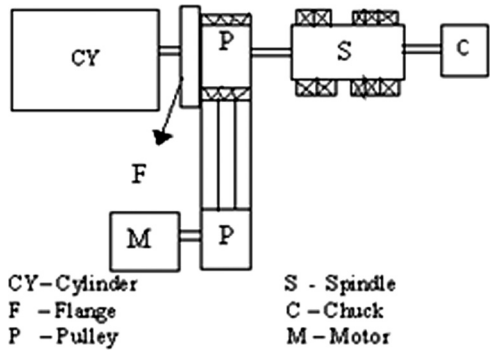

Fig. 7 Experimental setup

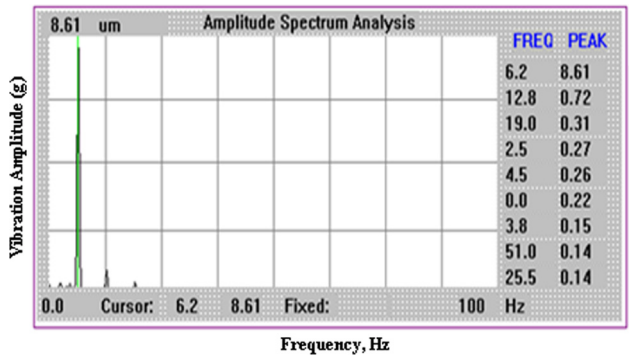

Fig. 8 Waveform of LGB – H before balancing

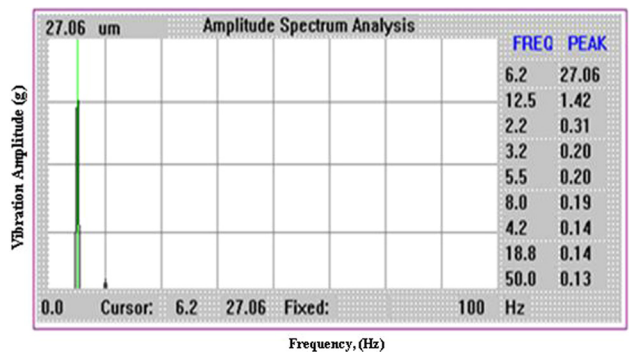

Fig. 9 Waveform of UGB –H before balancing

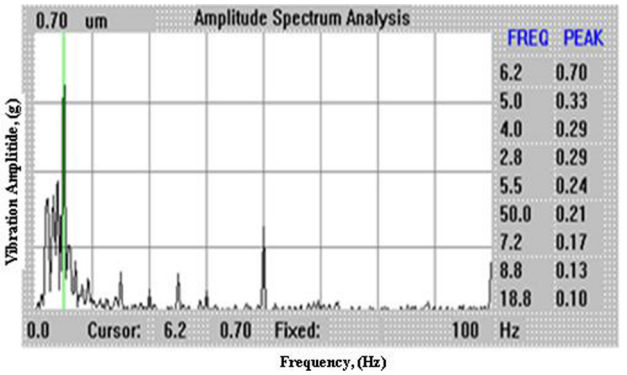

Fig. 10 Waveform of LGB – H after adding weight

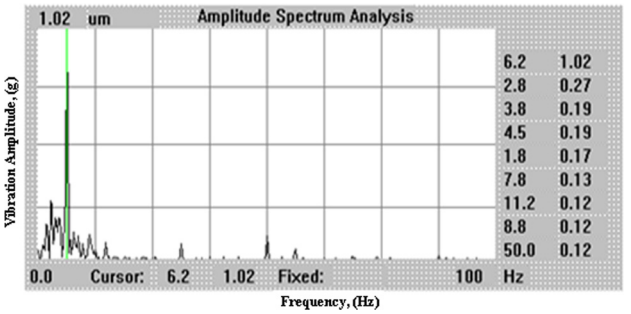

Fig. 11 Waveform of LGB after adding correction weight

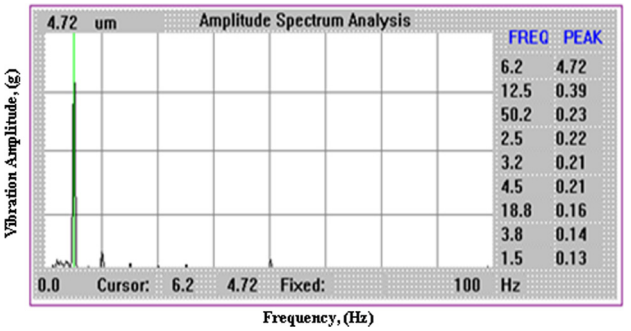

Fig. 12 Waveform at LGB after adding trial weight

housing of the test bearing. The accelerometer is connected to the FFT analyzer, the output of which is connected to a computer. The relevant hardware and the software required to acquire the data, store it, and display the time domain signal are installed in the computer used for this work.

For Fig. 7 the test bearing details are bearing No. 22,226 KM/W33/C3 SKF Sweden (double roller taper), sleeve No. H3126 (spherical roller bearing), pedestal No. SN 526, 2 numbers each, quantity 2 numbers.

6.1 Initial Machine Condition and Observation. The experimental work was carried out on a real time turbine generator machine of the sugar factory. The turbine generator (130 MW) was shutdown for nearly 3 months between (June 5, 2012) and (September 8, 2012) and such a rotating machine was selected. On September 8, 2012, the experiments were conducted during trial run and the lower guide bearing (LGB) vibration reading was found to be very high as per the FFT vibration and on-line vibration monitoring systems at a level of 190 and 7.5 microns, respectively. Detailed vibration analysis was carried out on UGB, LGB, and TGB with the help analyzer balancer with the FFT analysis, and it was found that one time speed vibration was predominant.

The high value of one time speed of vibrations at LGB and UGB were due to the imbalance in the rotor component of the generator. Hence it was decided to go for a single plane balancing of the rotor of the generator.

The online monitoring system readings on LGB after balancing, at no load were about 1.5 mils. So it was decided to excite the generator.

Then the generator was gradually loaded to full load. The online vibration readings at LGB was 3.2 mils.

On stabilized load condition, which is the normal working condition of the machine, the imbalance component of vibration, was brought down from 8.271 μm and 25.69 μm to 0.636 μm and 1.454 μm, respectively, in the LGB and UGB. The final vibration readings were also less than the permissible limits. Hence it was

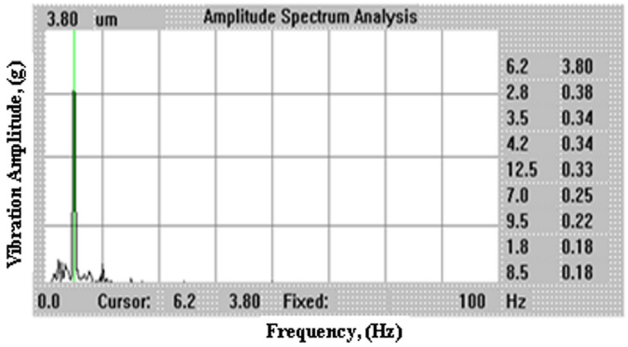

Fig. 13 Waveform of UGB after balancing at full load

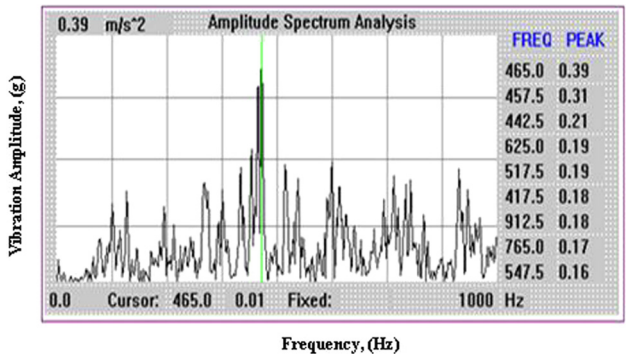

Fig. 14 Waveform at TGB on full load

decided that the generator is balanced to the optimum level and no further balancing is required These residuals in Figs. 8–14 clearly show that the amplitudes of displacement, velocity, and acceleration are increases due to the effect of unbalance and defective bearings.

6.2 Results of Dimensional Analysis of Experiments. Mathematical analysis with partial correlation integral analysis is used to analyze bearing vibration data collected throughout the lifetime of a bearing in test setup without any maintenance intervention. Although the system is under the influence of a relatively severe imbalance in the shaft and misalignment in the bearing supports, the analysis successfully shows the development of the defects in the bearing. These investigations reveal that first an inner-race defect is formed in the bearing together with a slight ball/roller defect. The dimensional analysis measures could be easily calculated and evaluated by maintenance technicians. If there is a need for further consultation and investigation, a detailed frequency-based spectral technique could be applied by an expert. From the numerical results presented in this paper, it is believed that the presented technique may accurately predict the dynamic characteristics of an antifriction bearing subjected to speed and loads.

Another important application of this model is system health monitoring. One of the most widely seen bearing failure cases is point defects on the contact surfaces, including the moving race, fixed race, and roller surfaces. Assuming medium-to-large defect size, the point defects have been formulated in Eq. (21). This formula, together with contact angles defined numerically and implemented to explore the defect prognosis. However, the location of the defect on the races is critical for the frequency response. For instance, if the defect is located at the center of the loading zone, the bottom of the outer race, every roller will hit it while going through the loading zone and will result in an overwhelmingly dominant frequency at the roller passing frequency. On the other hand, if the defect on the outer race is located at the top of the race, the rollers will mostly miss the point defect, and thus shift the dominant frequency to much lower bands.

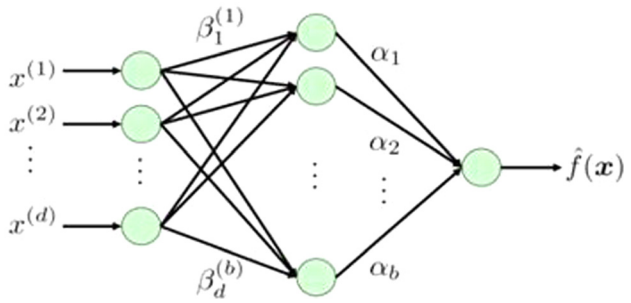

Fig. 15 Structure of three layered neural network

6.3 Artificial Neural Network Modeling. In recent times, the application of artificial intelligence techniques is increasing tremendously in almost all engineering areas. Modeling and optimization are necessary for the understanding and control of any process. Precise control is a prerequisite to achieve improved quality and productivity. Artificial neural network plays an important role in predicting the linear and nonlinear problems in different fields of engineering. Many attempts have been made of the multilayer Perceptron.

A multilayer Perceptron trained with the back-propagation algorithm may be viewed as a practical way of performing a linear input–output mapping of a general nature (Fig. 15). Back-propagation neural networks are usually referred to as feed forwarded, multilayered network with a number of hidden layers trained with a gradient descent technique. This algorithm is based on the error correction learning rule. Basically, the error back-propagation process consists of two passes through the different layers of the network, a forward pass and a backward pass. In the forward pass, an activity pattern (input vector) is applied to the sensory nodes of the network, and its effect propagates through the network layer by layer. Finally, a set of outputs is produced as the actual response of the network. During the backward pass, all synaptic weights are adjusted in accordance with the error correction rule. Specifically, the actual response of the network is subtracted from the desired (target) response to produce an error signal. The synaptic weights are adjusted so as to make the actual response of the network move closer to the desired network.

6.4 Simulation Procedure. The objective of the simulation was to first have the system learn the appropriate mappings between input and output variables by observing the training samples. The trained system was then used to determine the input conditions that maximize vibration amplitude (A) subject to certain constraints. The three-layer back-propagation with four inputs, two outputs, and nine hidden nodes was employed for the neural network. The network was trained using 54 samples that span the allowable ranges of input variables. The inputs were defects (nd), Load (W), number of rollers/balls (Z), speed (N), and outputs were amplitude (A) and frequencies (f). A random generator was used to initialize the values of the learning parameter. In order to decide on the structure of the neural network, the rate of error convergence was checked by changing the number of hidden layers and also by adjusting the learning rate and momentum rate. As a result, a neural network with nine neurons in the hidden layer was adopted for storing knowledge in the form of weights between neurons. A crucial problem in back-propagation is its generalization ability. There is no certainty that the network successfully trained on the given samples provides desired input/output associations for an untrained pattern as well. As the number of neurons increases, the approximation for weight will increase, and as a result we get an overfitted network model,

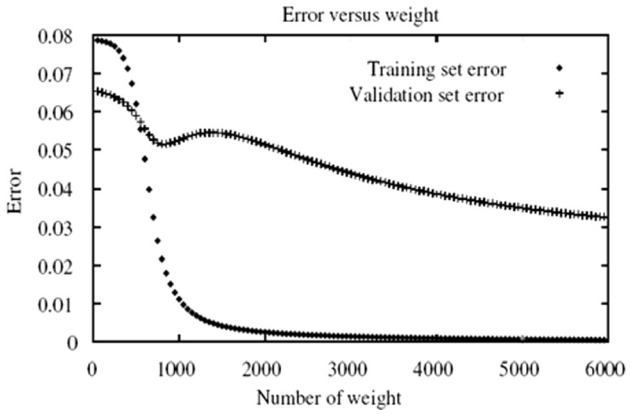

Fig. 16 Number of weight versus error

whereas for lesser number of neurons in the hidden layer are not capable to give the desired result. Therefore, it is necessary for any neural network that the number of neurons in the hidden layer should be appropriate. It is seen that 85% of the case single neuron is enough and the other 15% of the cases, two neurons are needed to train any neural network to get a good result.

It is clear from Fig. 16 that as we increase the weight, the ANN model in spite of interpolating the function, memorizes the result due to this error and increases on validating the model.

6.5 Validation of Model. The measurements are collected at different points, all in machine bearing housings, to detect various types of defects as shown in Fig. 2. Also, vibrations are measured along axial, horizontal, and vertical directions. Vibration signals are collected by means of a closed, proprietary vibration analyzer equipped with a sensor in the frequency domain and vibration signal techniques were applied within the system. There are a number of factors that contribute to the complexity of the bearing signature that could not be simulated but must be taken into consideration. Only with real data it is possible to work under real environment conditions. We will show and analyze some real examples to illustrate how the theory appears in practice. First of all, variations of the bearing geometry and assembly make it impossible to precisely determine bearing characteristics frequencies. The fault severity progress can alter the bearing geometry, contributing to the increase in complexity of the diagnosis process. Operating speed and loads of the shaft greatly affect the way and the amount a machine vibrates causing bearing basic frequencies to deviate from the calculated value.

For the developed setup and the data from the ANN process carried out on the setup, a dimensional analysis of the process was developed. Considering the different parameters having an effect on the amplitude of vibrations, an equation was developed from regression analysis with origin software. To validate the model, further experiments were carried out and the observed values of experiment were plotted with the values estimated from the equation obtained from regression analysis. The relative curve we get through experimentally and theoretically are almost showing the same behavior as shown in Fig. 15. This model can be utilized for the ANN process, where the amplitude and frequencies obtained is a function of the listed parameters. It is clear from the results that the neural network model is better than the regression model because its results are quite nearer to the actual result, whereas the regression model is performing better only if the R^2 value is high, near 100%. ANN modeling consumes less time with a high degree of accuracy. Hence, it can be concluded that ANN is highly effective for predicting defects and vibration amplitudes.

Overall, the defect on the inner race causes quite a chaotic system response characterized by a lot of frequency spikes in broad band and significantly increased displacement and force response magnitudes. This is consistent with observations obtained from the study of the experimental data based models, which reveals that the surface defects on the moving race (inner race) tends to cause more complicated dynamic behaviors with enriched resonant frequency pool. The distinct characteristic frequencies are the cage passing frequency with respect to the inner race, observed in the horizontal and vertical displacement responses, respectively. These phenomena can potentially be applied to distinguish the moving race defect from the moving race surface waviness.

Table 11 Vibration readings

Speed	C.S.		N.C.S.	
rpm	*H* (g)	*V* (g)	*H* (g)	*V* (g)
500	0.67	0.87	0.82	0.99
1000	0.44	0.99	0.70	0.34
1500	0.690	0.988	0.74	0.257
2000	2.14	2.55	0.639	0.819

The size of the point defect is similar to the inner race point defect in Fig. 2. For vertical displacement and force, the point defect on the outer race increases the response magnitude by one order without significantly altering the amplitude frequency pattern. The most dominant frequencies are the roller passing frequency and its super harmonics. To investigate the influence of the defect on the roller surface, it is assumed that we have a defect on the roller. As shown by Eq. (21), the defect on the roller illustrates more dramatic impacts on the axial displacement, while only showing effects on the vertical and horizontal displacement. For the horizontal displacement, the shaft frequency disappears as a dominant frequency. Similar to the defects on the inner and outer races, the defect on the roller surfaces causes increased vertical forces response in a broad band. The vibration signature of Fig. 4 shows the existence of multiples of the rolling bearing cage characteristic frequency indicating that the bearing condition is critical.

6.6 Case Studies. Case study on condition monitoring vibration analysis and dynamic balancing of a CNC M/C (turning center) spindle. Dynamic balancing of the critical machinery to ensure the vibration is minimized to the maximum possible extent for better productivity and performance of the respective machines.

Keeping the vibrations within the limits, particularly the spindle of CNC machinery helps in achieving:

- faster cutting speeds
- longer tool life
- better surface finishing
- longer life of the spindle and bearings of the spindle
- noise reduction
- breakages prevention
- longer machine life with better performance

Below is a small case study involving the vibration analysis of the CNC machine model Spinner 15 of Askar Microns Pvt., Limited – Pune, which demonstrates the application of vibration analysis and dynamic balancing as a concept in reducing the spindle vibrations to a minimum possible level. The vibration analysis and dynamic balancing was carried out in three levels as follows:

Level I: Motor and its Pulley. Vibration analysis was carried out on the motor-pulley and was found to be well bearing frequencies with minimum vibration levels.

Level II. Total assembly - motor, pulley connected to the spindle, pulley, flange, and cylinder, and chuck. Vibration analysis was carried out and was found that, at spindle rotational speed of 2000 rpm the vibration level was very high in the chuck side. The FFT spectrum at chuck side reveals that bearing frequency was

Table 12 Vibration readings

Level II	H (g)	V (g)
Before changing the bearing	2.14	2.55
After changing the bearing	0.13	0.15

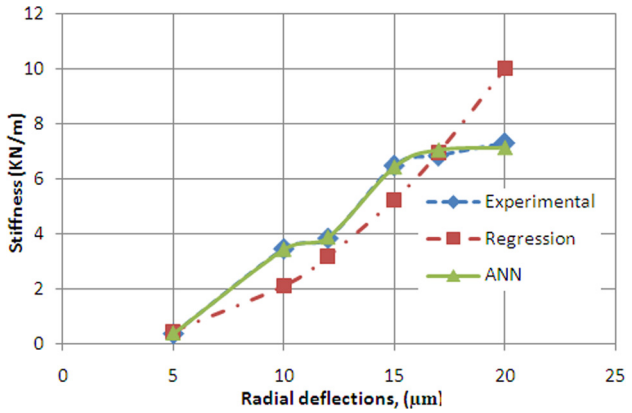

Fig. 17 Deflection versus stiffness

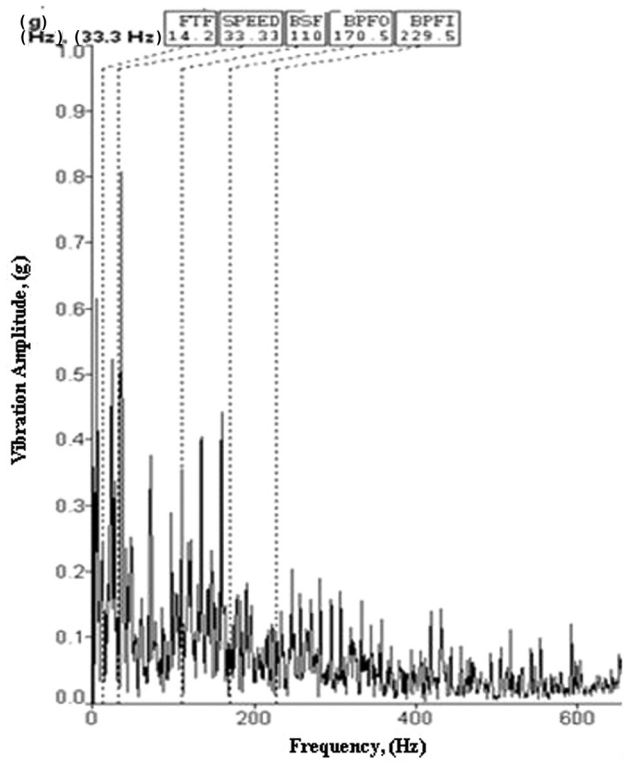

Fig. 18 Damaged bearings

found high in g. The vibration values at various speeds have been measured, both on the chuck and nonchuck side as mentioned below, which are given in Table 11.

We checked the bearings at chuck side, and out of the three bearings one of them was found to be a failure Apart from that failure vibration value was found high at 2000 rpm and slightly high at 1500 rpm. The FFT spectrum has been shown in Fig. 18, before changing the bearing, the bearing frequencies are high. After changing the bearing, the reduction in overall vibration level

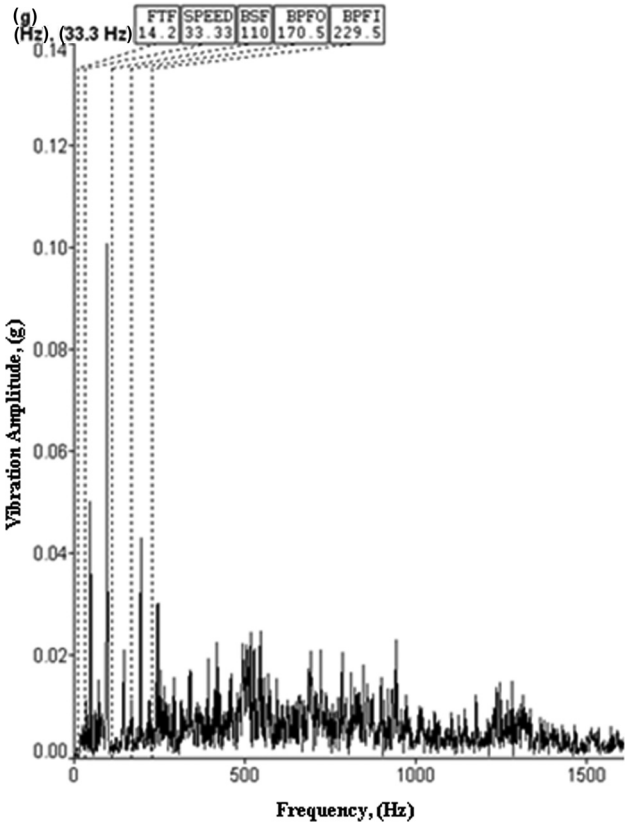

Fig. 19 Healthy bearings

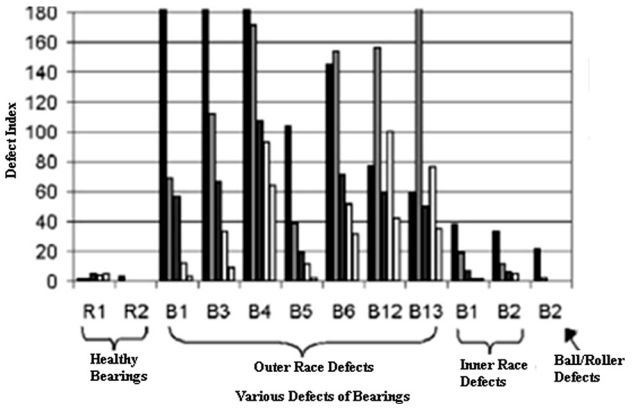

Fig. 20 Defective bearings produce significantly more fault-index than healthy bearings

in the chuck side was found. The vibration readings have been measured after changing the bearing, which is given in Table 12.

Level II has resulted in very low vibration values of the spindle because of changing the bearing at the chuck side of the cartridge as a whole assembly. This reduced vibration of the CNC machine will give a very accurate surface finish of the machined product and this automatically results in the improvement of the quality of the product (Fig. 17).

Figure 18 shows that in the spectrum as a narrow band spike or as a sum or difference frequency. When more than one roller is defective, sums of the ball spin frequency can be generated. The number of sums is equal to the number of defective rollers. The ball spin frequency could be generated if the cage is broken, and if the balls are thrusting hard against the cage. Normally, defects on the balls or rollers are accompanied by a defective

inner race and/or outer race. To validate the model, further experiments were carried out and the observed values of the experiment were plotted (Figs. 19 and 20) with the values estimated from the equation obtained from dimensional analysis (Eq. (21)). The relative curve we get through experimentally and theoretically are almost showing the same behavior as shown in Figs. 18 and 19 similar to Fig. 5.

7 Concluding Remarks

In conclusion, the study shows that the use of the EDBM of the vibration signature can provide an effective procedure in identifying and quantifying bearing damage for prognostication application. The present study may be summarized as follows:

The use of frequency spectrum analysis provides an indication of component failure with the existence of large side band components. It can also provide some information concerning the degree of damage without any specific indication of types of failure.

For roller element failure, if the damage location did not make contact with the races during the sampling time window, the damage cannot be detected in the frequency spectrum on any type of time analysis. The use of the EDBM with vibration data can assure the contact of the damage.

The use the EDBM can provide a dependable identification of the type of damage (the number of peaks equals to the number of roller elements using relative speed can provide identification of damage in the bearing race while damage in the roller elements will provide an significant increase in vibration amplitude) as well as an accurate quantification of the damage level in rolling element bearings.

The use of the EDBM based on the shaft speed can provide a good identification of the location of the damage with reference to the shaft reference point. The use of the EDBM based on the relative speed can provide a better identification of the damage type and its level than those based on the shaft speed of the bearing. Based on the results from this study an interpolating algorithm can used to relate vibration amplitudes with bearing surface pitting and depth (pitting volume as failure criteria provided by bearing manufacturers).

For the developed setup and the data from the ANN process carried out on the setup, a dimensional analysis of the process was developed. To validate the model, further experiments were carried out and the observed values of experiment were plotted with the values estimated from the equation obtained from regression analysis. The relative curve we get through experimentally and theoretically are almost showing the same behavior.

8 Scope for Future Work

In the future, an attempt will be made to understand the structural damage through experimental data based model analysis. To automate a process, input-output relationships are to be known beforehand in both forward, as well as reverse directions. The authors are presently working on these issues [44–52].

Acknowledgment

The authors gratefully acknowledge the help and cooperation of Dr. R. A. Kanai, Executive Director, ADCET, Ashta, and Dr. S. G. Joshi, former Professor and Head, Department of Mechanical Engineering, Walchand College of Engineering Sangli, India, in carrying out the real experiments.

References

[1] Massimo, C., and Alberto, I., 2002, "Analysis of Damage Bearings of Aeronautical Transmission by Auto-Power Spectrum and Cross-Power Spectrum," ASME, J. Vibr. Acoust., **124**, pp. 180–185.
[2] Sebastian, V., Henning, Z., and Mario, P., 2007, "Rolling Bearing Condition Monitoring Based on Frequency Response Analysis," Diagnostics for Electric Machines, Power Electronics and Drives, IEEE International Symposium, pp. 29–35.
[3] Tandan, N., Yadava, G. S., and Ramakrishna, K. M., 2007, "A Comparison of Some Condition Monitoring Techniques for the Detection of Defect in Induction Motor Ball Bearing," Mech. Syst. Signal Process., **21**, pp. 244–256.
[4] Langhaar, H. L., 1951, *Dimensional Analysis and Theory of Models*, Wiley, New York.
[5] Patel, V. N., Tandan, N., and Pandey, R. K., 2010, "A Dynamic Model for Vibration Studies of Deep Groove Ball Bearings Considering Single and Multiple Defects in Races," ASME J. Tribol., **132**, p. 041101.
[6] Patil, M. S., Mathew, J., and Desai, S., 2010, "A Theoretical Model to Predict the Effect of Localized Defect on Vibrations Associated With Ball Bearings," Int. J. Mech. Sci., **52**, pp. 1193–1201.
[7] Shuang, L. V., 2007, "Rolling Bearings Fault Diagnosis Based on Wavelet-Neural Network," IEEE International Technology and Innovation Conference, pp. 1884–1887.
[8] Arslan, H., and Akturk, N., 2008, "An Investigation of Rolling Element Vibrations Caused by Local Defects," Trans. ASME, J. Tribol., **130**, p. 041101.
[9] Roque, A. A., Silva, T. A. N., and Dias, J. C. Q., 2009, "An Approach to Fault Diagnosis of Rolling Bearings," WSEAS transactions on systems and control, Issue 4, 4, ISSN: 1991-8763, pp. 188–197.
[10] Choy, F. K., Zhou, J., and Braun, M. J., 2005, "Vibration Monitoring and Damage Quantification of Faulty Ball Bearings," Trans. ASME, J. Tribol., **127**, pp. 776–783.
[11] Tandan, N., and Choudhury, A., 1999, "A Review of the Vibration and Acoustic Measurement Methods for Detection of Defects in Rolling Element Bearings," Tribol. Int., **32**(8), pp. 469–480.
[12] Nakhaeinejad, M., Michael, M. D., 2011, "Dynamic Modeling of Rolling Element Bearings With Surface Contact Defects Using Bond Graphs," Trans. ASME, J. Tribol., **133**, p. 011102.
[13] Soylemezoglu, A., Jagannathan, S., and Can, S., 2010, "Mahalanobis-Taguchi System (MTS) as a Prognostics Tool For Rolling Element Bearing Failures," Trans. ASME, J. Manufacturing Sci. Eng., **132**(5), p. 051014.
[14] Wang, W. J., Wu, Z. T., and Chen, J., 2001, "Fault Identification in Rotating Machinery Using The Correlation Dimension and Bispectra," Nonlinear Dyn., **25**, pp. 383–393.
[15] Wei, H., and Xiang, Z., 2009, "Application of the Wavelet-SOFM Network in Roll Bearing Defect Diagnosis," IEEE, Computer Society, Global Congress on Intelligent Systems, pp. 8–12.
[16] Ihab, S., Ip-Shing, F., and Perinpanayagam, S., 2010, "Fault Diagnosis Of Rolling Element Bearings Using An EMRAN RBF Neural Network- Demonstrated Using Real Experimental Data," IEEE Sixth International Conference on Natural Computation (ICNC 2010), pp. 287–291.
[17] Huaqing, W., and Chen, P., 2011, "Intelligent Diagnosis Method For Rolling Element Bearing Faults Using Possibility Theory And Neural Network," IEEE Trans. Comput. Ind. Eng., **60**(4), pp. 511–518.
[18] Czeslaw, T., and Kowalski, T. O. K., 2003, "Neural Networks Application For Induction Motor Faults Diagnosis," Math. Comput. Simul., **63**, pp. 435–448.
[19] Hoffman, A. J., and Merwe, N. T., 2002, "The Application of Neural Networks To Vibrational Diagnostics For Multiple Fault Conditions," Comput. Stand. Interfaces, **24**, pp. 139–149.
[20] Chun-Chieh, W., and Yuan Kang, P. C. S., 2010, "Applications of Fault Diagnosis In Rotating Machinery By Using Time Series Analysis With Neural Network," Expert Systems With Applications, **37**, pp. 1696–1702.
[21] Yuh-Tay, S., 2009, "On the Study of Applying Morlet Wavelet to the Hilbert Transform for the Envelope Detection of Bearing Vibrations," Mech. Syst. Signal Processing, **23**, pp. 1518–1527.
[22] Sugumaran, K. I., and Ramchandra, K. I., 2011, "Fault Diagnosis of Roller Bearing Using Fuzzy Classifier and Histogram Features With Focus on Automatic Rule Learning," Expert Systems With Applications, **38**, pp. 4901–4907.
[23] Prabhakar, S., Mohanty, A. R., and Sekhar, A. S., 2002, "Application of Discrete Wavelet Transform For Detection of Ball Bearing Race Faults," Tribol. Int., **35**, pp. 793–800.
[24] Kunpeng, Z., Wong, Y. S., and Hong, G. S., 2009, "Wavelet Analysis of Sensor Signals For Tool Condition Monitoring: A Review and Some New Results," Int. J. Machine Tools & Manufacture, **49**, pp. 537–553.
[25] Singh, G. K., and Ahmed, S. Al. K., 2009, "Isolation and Identification of Dry Bearing Faults In Induction Machine Using Wavelet Transform," Tribol. Int., **42**, pp. 849–861.
[26] Ghafari, S. H., and Golnaraghi, F. I., 2008, "Effect of Localized Faults on Chaotic Vibration of Rolling Element Bearings," Nonlinear Dyn., **53**, pp. 287–301.
[27] Tao, B., Limin, Z., and Han, D., 2007, "An Alternative Time-Domain Index for Condition Monitoring of Rolling Element Bearings-A Comparison Study," Reliab. Eng. Syst. Safety, **92**, pp. 660–670.
[28] Mevel, B., and Guyader, J. L., 1993, "Routes to Chaos in Ball Bearing," J. Sound Vib., **162**(3), pp. 471–487.
[29] Chongsheng, L., and Liangsheng, Q., 2007, "Application of Chaotic Oscillator in Machinery Fault Diagnosis," Mech. Syst. Signal Processing, **21**, pp. 257–269.
[30] Shengping, F., Changle, X., and Jingyan, W., 2009, "Numerical Calculation of Ball Bearing Excitation and Application in Multi-Body Dynamics Simulation," Computer-Aided Industrial Design and Conceptual Design, IEEE 10th International Conference, pp. 596–600.
[31] McFadden, P. D., and Smith, J. D., 1984, "Model for the Vibration Produced by a Single Point Defect in a Rolling Element Bearing," J. Sound Vib., **96**(1), pp. 69–82.
[32] McFadden, P. D., and Smith, J. D., 1985, "Model for the Vibration Produced by a Multiple Point Defect in a Rolling Element Bearing," J. Sound Vib.,**98**(2), pp. 263–273.

[33] Meyer, L. D., Ahlgren, F. F., and Weichbrodt, B., 1980, "An Analytical Model for Ball Bearing Vibrations to Predict Vibration Response to Distributed Defects," ASME J. Mech. Design Trans., **102**, pp. 205–210.
[34] Tandan, N., and Choudhury, A., 1997, "An Analytical Model for the Prediction of the Vibration Response of Rolling Element Bearings Due to a Localized Defects," J. Sound Vib., **205**(3), pp. 275–292.
[35] Zeki, K., and Hira, K., 2006, "Vibration Analysis of Rolling Element Bearing With Various Defects Under the Action of an Unbalanced Force," Mech. Syst. Signal Process., **20**, pp. 1967–1991.
[36] Przemyslaw, S., and Tomasz, K., 2005, "A Model for the Determination of the Resisting Torque of the Rolling Bearing Cage Motion of Slow-Speed Kinematic Pairs," Meccanica, **40**, pp. 35–47.
[37] Prasad, H., 2002, "Relative Comparison of Stiffness and Damping Properties of Double Decker High Precision and Conventional Rolling-Element Bearings," Tribol. Int., **35**, pp. 265–269.
[38] Bin, W., and Minjie, W., 2007, "An Approach of Bearing Fault Detection and Diagnosis at Varying Rotating Speed," IEEE International Conference on Control and Automation, pp. 1634–1637.
[39] Upadhyay, S. H., Harsha, S. P., and Jain, S. C., 2008, "Nonlinear Vibration Signature Analysis of High Speed Rotor Due To Defects Of Rolling Element," Adv. Theor. Appl. Mech., **1**(7), pp. 301–314. Available at: http://m-hikari.com/atam/atam2008/atam5-8-2008/upadhyayATAM5-8-2008.pdf
[40] Purohit, R. K., and Purohit, K., 2006, "Dynamic Analysis of Ball Bearings With Effect of Preload and Number of Balls," Int. J. Appl. Mech. Eng., **11**(1), pp. 77–91. Available at: http://www.ijame.uz.zgora.pl/ijame_files/archives/v11PDF/n1/77-91_Article_05.pdf
[41] Wentao, S., and Zhang, D., 2011, "Research on Envelope Analysis for Bearings Fault Detection," 5th International Conference on Computer Science and Education, Hefei, China, August 24-27, pp. 973–976.
[42] Fidel, E. H., and Oscar, C. M., 2008, "The Application of Bispectrum on Diagnosis of Rolling Element Bearing: A Theoretical Approach," Mech. Syst. Signal Process., **22**, pp. 588–596.
[43] Zubrenkov, B. I., and Sen'kina, V. V., 2010, "Modal Analysis of the Structure of Rotating Machines With Roller Bearings," ISSN 1068–798X, Russian Engineering Research, **30**(5), pp. 442–445.
[44] Harris, T. A., 2001, *Rolling Bearing Analysis*, 4th ed., Wiley-Interscience, New York, NY.
[45] Eschmann, P., 1985, *Ball and Roller Bearings-Theory, Design, and Application*, Wiley, New York.
[46] Gupta, P. K., 1984, *Advanced Dynamics of Rolling Elements*, Springer-Verlag, New York.
[47] Changsen, W., 1991, *Analysis of Rolling Element Bearings*, Mechanical Engineering Publications Ltd., London.
[48] Rao, J. S., 2000, *Vibratory Condition Monitoring of Machines*, Narosa, New Delhi.
[49] Hamrock, B. J., 1994, *Fundamentals of Fluid Film Lubrication*, Mechanical Engineering Series, McGraw-Hill Editions, Singapore.
[50] Ragulskis, K., and Yurkauskas, A., 1989, *Vibrations of Bearings*, Applications of Vibration Series, Hemisphere Publishing Corporation, New York.
[51] Taylor, J. I., 1994, *The Vibration Analysis Handbook*, Vibrations Consultants Inc., 360 pages.
[52] Harris, T., and Kotzalas, M., 2007, *Essential Concepts of Bearing Technology*, Taylor & Francis, Boca Raton, FL.